On the use of the material point method to model problems involving large rotational deformation

L. Wang, W.M. Coombs & C.E. Augarde
Department of Engineering, Durham University, Durham, UK

M. Brown, J. Knappett, A. Brennan & C. Davidson
School of Science & Engineering, University of Dundee, Dundee, UK

D. Richards & A. Blake
Faculty of Engineering and the Environment, University of Southampton, Southampton, UK

ABSTRACT: The Material Point Method (MPM) is a quasi Eulerian-Lagrangian approach to solve solid mechanics problems involving large deformations. In order to improve the stability of the MPM, several extensions have been proposed in the last decade. In these extensions, the sudden change of stiffness when a point crossing an element boundary in the standard MPM is avoided by replacing a material point with a deformable particle domain. The latest extensions are Convected Particle Domain Interpolation approaches, primarily including the CPDI1 and recently published CPDI2. We have unified the standard MPM and CPDI approaches into one implicit computational framework, and here investigate their ability to model problems involving large rotational deformation, which is essential in the installation of screw pile foundations. It was found that the CPDI2 approach can produce erroneous results due to particle domain distortion, while the CPDI1 approach and standard MPM can predict more physically realistic mechanical responses.

1 INTRODUCTION

The Material Point Method (MPM) is a numerical method used to simulate massive deformation of solids combining advantages of both Eulerian and Lagrangian approaches for solving solid mechanics problems. In the MPM a body is described by a number of Lagrangian material points, at which state variables are stored and tracked. Computation for an incremental loading is then carried out on a background computational mesh. As demonstrated in Figure 1 for a simple shear problem, the total deformation and other state variables are stored at the material points, while the background mesh is extended with the incremental displacment, thus avoiding the mesh distortion seen with the standard FEM for large deformation problems. In fact, the background mesh can be any mesh at the beginning of each load step. Because of this attraction the MPM has been applied to several large deformation problems particularly in the area of geotechnical engineering, e.g. (Ceccato et al. 2016, among others).

As part of wider study, we are developing a program based on the MPM to model the soil response to the installation of a screw pile, with the engineering application of providing a computer-aided design tool for engineers to optimise pile design for offshore wind turbine foundations (Wang et al. 2017). During installation of a screw pile, the pile is pushed and rotated into the ground. Our program focuses on computation of the vertical force and torque applied on the pile for this installation. Modelling large torsion

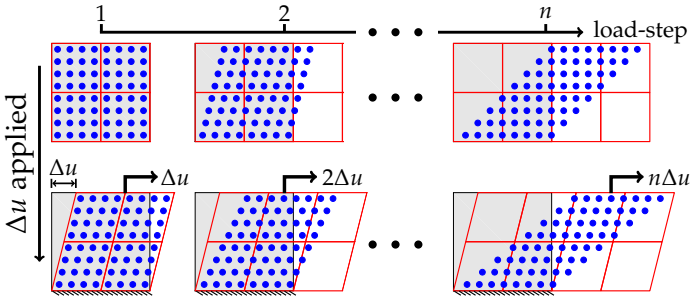

Figure 1: Demonstration of the standard MPM under simple shear: a high quality mesh (red) is used in the computation of equilibrium for each loading increment, while the material points (blue) track the total deformation.

is essential for this purpose.

The method of mapping the state variables back and forth between the material points and background mesh nodes in the MPM is a crucial step. For example, in a static elasticity analysis, the stresses at material points are used to work out the nodal internal force; and a material point's position is updated by adding incremental displacements interpolated from the nodal increment displacements. In the *standard MPM (sMPM)*, a material point only relates to its *parent element*, (i.e. the backgound element in which it is currently located). However, the sMPM has an inherent instability when a material point crosses an element boundary. This instability is due to the sudden transfer of stiffness between elements, this can result in some elements having very little stiffness, or some internal elements losing all stiffness. Therefore, several extensions to the sMPM have been proposed,

each of which replace the material point with a deformable particle domain. The most notable of these extensions are the *Generalized Interpolation Material Point (GIMP)* (Bardenhagen and Kober 2004), *Convected Particle Domain Interpolation (CPDI1)* (Sadeghirad et al. 2011), and *Second-order CPDI (CPDI2)* (Sadeghirad et al. 2013). Assigning a particle domain to each material point enables the influence domain of a material point to cover more than one element. For a 2D problem, the particle domain is a rectangle in GIMP, a parallelogram in CPDI1 and a quadrilateral in CPDI2. Therefore, the CPDI2 approach has particle domains for completely covering a general body, while are gaps or overlaps with the other two approaches. Previously, these methods have not been examined in terms of their ability to model problems involving large rotational deformation, and this is the focus of this paper.

Applying boundary conditions is another challenge when using the MPM, because the mesh is independent of the probem domain (unlike in the FEM) and the domain boundary generally is not included in the computational mesh. This is probably why numerical examples in many published papers consider problems in which body forces only are present. With a regular grid as the computational mesh, Dirichlet boundary conditions can be applied using the implicit boundary method, e.g. Cortis et al. (2017). However, in our project the geometry of a screw pile is more complex than allowed for in that paper. In this framework, the *moving mesh concept* (Beuth 2012), which simply modifies the computational mesh such that the boundary of domain is explicitly included in the mesh, is adapted as the rotating mesh associated with the rotation, as detailed in Wang et al. (2017). In order to generate mesh including body boundary, an unstructured mesh is used. With the mesh including the domain boundary at the beginning of each load-step, boundary conditions are applied on these mesh nodes, straightforwardly as in the FEM.

In this paper, the sMPM and CPDI approaches are unified into one computational framework. This framework solves a quasi-static problem for the deformation of elasto-plastic material. The finite stain theory is used to characterise the deformation. The plastic yield condition is governed by the von-Mises criterion. An implicit stress return algorithm is employed for finding the stress state after material is yielded, such that the yield condition is accurately enforced, with more details included in Coombs (2011). An implicit scheme is also employed for solving the system of equations. This allows large load-steps and increases in stability and accuracy, as shown in Charlton et al. (2017).

This unified computational framework is verified and investigated for modelling large torsion. The performance of these methods is compared in Section 3 and conclusions are drawn in Section 4.

2 COMPUTATIONAL FRAMEWORK

This computational framework solves implicitly the weak form of the equilibrium eqution for the quasi-static finite deformation problem of an elasto-plastic material. The formulation is largely based on Charlton et al. (2017) but uses different particle domains and basis functions, which are detailed below.

Compared to the FEM, the MPM requires mapping between material points and the computational mesh. However, the computation inside each load-step, e.g. each column in Figure 1, is the same as in the FEM. Therefore, we present a unified computational framework for integrating the standard material point methods and the CPDI approaches as follows.

(i) Set up problems: generate computational mesh, specify boundary conditions and material parameters, and generate

- IF (sMPM): material point coordinates
- IF (CPDI1): material point coordinates and two vectors, ($\boldsymbol{s}^0$, $\boldsymbol{t}^0$), of the parallelogram particle domain for each material point
- IF (CPDI2): corners and connectivity for the particle domains

and material point volumes.

(ii) A load-step starts, incremental boundary conditions are specified.

(iii) Find influence elements of material points in the mesh:

- IF (sMPM): FOREACH material point, p, find its parent element
- IF (CPDI1): FOREACH material point, p, to compute the coordinates of four corners of its particle domain as

$$\boldsymbol{x}_p + [-1 \;\; 1 \;\; 1 \;\; -1]\frac{\boldsymbol{s}_p}{2} + [-1 \;\; -1 \;\; 1 \;\; 1]\frac{\boldsymbol{t}_p}{2}$$

  and find parents elements for these corners
- IF (CPDI2): FOREACH corner to find its parent element

(iv) Compute the *basis functions* S_{ip} and their *spatial gradients* ∇S_{ip} for node i and material point p: FOREACH material point apply the following:

- IF (sMPM)

$$S_{ip} = S_i(\boldsymbol{x}_p), \qquad \nabla S_{ip} = \nabla S_i(\boldsymbol{x}_p),$$

  where $S_i(\bullet)$ are the standard FEM basis functions and $\boldsymbol{x}_p$ are the coordinates of material point p.

- IF (CPDI1)

$$S_{ip} = \frac{1}{4}\left[S_i(\boldsymbol{x}_p^1) + S_i(\boldsymbol{x}_p^2) + S_i(\boldsymbol{x}_p^3) + S_i(\boldsymbol{x}_p^4)\right],$$

$$\nabla S_{ip} = \frac{1}{2V_p}\left\{\left(S_i(\boldsymbol{x}_p^1) - S_i(\boldsymbol{x}_p^3)\right)\begin{bmatrix} s_y - t_y \\ t_x - s_x \end{bmatrix} + \left(S_i(\boldsymbol{x}_p^2) - S_i(\boldsymbol{x}_p^4)\right)\begin{bmatrix} s_y + t_y \\ -s_x - t_x \end{bmatrix}\right\},$$

where the superscript indicates the index of particle domain corners.

- IF (CPDI2)

$$S_{ip} = \frac{1}{24v_p}\left[(6v_p - a - b)S_i(\boldsymbol{x}_p^1) + (6v_p - a + b)S_i(\boldsymbol{x}_p^2) + (6v_p + a + b)S_i(\boldsymbol{x}_p^3) + (6v_p + a - b)S_i(\boldsymbol{x}_p^4)\right],$$

$$\nabla S_{ip} = \frac{1}{2V_p}\left\{S_i(\boldsymbol{x}_p^1)\begin{bmatrix} y_p^2 - y_p^4 \\ x_p^4 - x_p^2 \end{bmatrix} + S_i(\boldsymbol{x}_p^2)\begin{bmatrix} y_p^3 - y_p^1 \\ x_p^1 - x_p^3 \end{bmatrix} + S_i(\boldsymbol{x}_p^3)\begin{bmatrix} y_p^4 - y_p^2 \\ x_p^2 - x_p^4 \end{bmatrix} + S_i(\boldsymbol{x}_p^4)\begin{bmatrix} y_p^1 - y_p^3 \\ x_p^3 - x_p^1 \end{bmatrix}\right\},$$

where

$$a = (x_p^4 - x_p^1)(y_p^2 - y_p^3) - (x_p^2 - x_p^3)(y_p^4 - y_p^1),$$

$$b = (x_p^3 - x_p^4)(y_p^1 - y_p^2) - (x_p^1 - x_p^2)(y_p^3 - y_p^4).$$

For more detail on these basis functions see (Sadeghirad et al. 2013).

(v) The nodal internal force can then be obtained from the stresses at the material point using

$$\boldsymbol{f}_i^{int} = -\sum_p \nabla S_{ip}\boldsymbol{\sigma}_p v_p,$$

where $\boldsymbol{\sigma}_p$ is the Cauchy stress and v_p the volume of the material point p. The system of equations for the nodal force equilibrium can then be formed

$$\boldsymbol{f}^{int} - \left(\boldsymbol{f}^{rea} + \boldsymbol{f}^{ext}\right) = \boldsymbol{0}, \tag{1}$$

where the superscripts rea and ext indicate nodal reactions and external forces.

(vi) Solve (1) with the Newton-Raphson (NR) iterative solver to obtain the nodal incremental displacement.

(vii) Map nodal incremental displacements onto the material points, and added onto the total displacement field as

$$\boldsymbol{x}_p = \boldsymbol{x}_p + \Delta\boldsymbol{u}_p = \boldsymbol{x}_p + \sum_i S_{ip}\Delta\boldsymbol{u}_i.$$

for the sMPM and CPDI1 approach. For the CPDI2 approach, the corners of particle domains are updated in the same manner. Other state variables, e.g. deformation gradient $\mathbf{F}$ and Cauchy stress, are also updated. In addition, the particle volume are updated:

- IF (sMPM): v_p=$v_p^0 \det \mathbf{F}_p$, where superscript 0 indicates a value in the initial configuration
- IF (CPDI1): $\boldsymbol{s}_p$=$\mathbf{F}_p\boldsymbol{s}_p^0$, $\boldsymbol{t}_p$=$\mathbf{F}_p\boldsymbol{t}_p^0$, and $v_p = |\boldsymbol{s}_p \times \boldsymbol{t}_p|$
- IF (CPDI2): v_p is the volume of particle domain with updated corners

(viii) The computational mesh is simply modified by the moving mesh concept and go back to (ii) for simulation of next load-step.

Employing an unstructured mesh, the cost in step (iii) for finding the position in a mesh for a point is increased, because it cannot be determined by computing the offset as with a structured mesh. Instead, a searching routine has be to used by looping over elements for a point. However, the independence of the job of checking whether a point is inside of the an element for different points and different elements enables us to parallelise these loops and speed-up computation in this framework. The searching algorithm can be further speeded up by reducing the searching region with a assistant bucket data structure, e.g. a multilevel octree bucket in Nie et al. (2012).

3 NUMERICAL EXAMPLES

The computational framework is first validated through benchmark problems. The performance of all the methods are then investigated for a problem involving large rotational deformation.

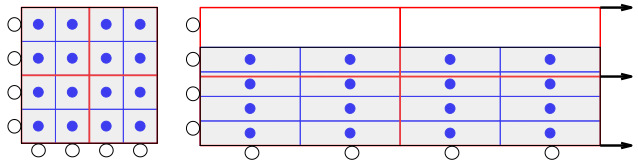

Figure 2: Left: Initial geometry (grey), computation mesh (red), material points and particle domains (blue) with roller boundary conditions in the CPDI2 approach. Right: deformed geometry (grey) subject to uni-axial stretch and plane-strain condition.

3.1 *Validation*

The simple stretch of a square block is simulated by the FEM, sMPM and CPDI approaches under the plane-strain condition. The block has dimension 2×2 with the elasto-plastic material, specified by the von-Mises constitutive law, with the yield criterion

$$\rho = \sqrt{2J_2}/\rho_c - 1,$$

where J_2 is the second invariant of the deviatoric part of the Kirchhoff stress tensor. The material parameters are Young's modulus $E = 1000$, Poisson's ratio $\nu = 0$ and yield strength $\rho_c = 400$. All variables have compatible units.

For the FEM case, the block was discretised by four bi-linear quadrilateral elements. For other cases, the same mesh was used with four material points per element. Figure 2 shows the geometry, mesh and boundary conditions for the CPDI2 approach in both initial and deformed configurations. Roller boundary conditions were applied on the bottom and left sides, with a horizontal displacement of 0.2 per load-step applied on the right. The simulation was run up to 20 steps. Due to the moving right boundary and displacement applied there, the moving mesh concept described above was adopted such that the computed incremental horizontal displacement was applied to the mesh at the end of each load-step.

Quadratic convergence rate of solver for the global equilibrium is expected, since the nonlinear system of equations are solved by the NR iteration. The convergence of the CPDI2 approach is shown in Figure 3 by plotting the residual, i.e. L_2 norm of the left hand side of (1), against the NR iteration steps in each load-step. Particularly, the residual of an iteration against that of the previous iteration shows that the average convergence rate is 1.996. The sMPM and CPDI1 approach also have this correct quadratic convergence rate.

The x-component of reaction force on the right end from the sMPM and FEM are plotted in Figure 4, where the markers show the load-steps. The force increases non-linearly in the first six steps due to the large deformation mechanics, i.e. the geometric non-linear finite strain measure used in the computational framework. In the seventh step, the material yields and so this reaction force starts to decrease gradually. The results from the sMPM and CPDI approaches are the same with the FEM, as this FEM simulation is not affected by mesh distortion. This agreement validates the computational framework and computer codes of the sMPM and CPDI approaches.

3.2 *Doughnut twist*

To test the formulations performances for large torsion problems, a challenging problem, used involving the azimuthal shear of a confined annular domain, is termed the Doughnut Twist problem here. The geometry, boundary conditions and material parameters of this problem are shown in Figure 5.

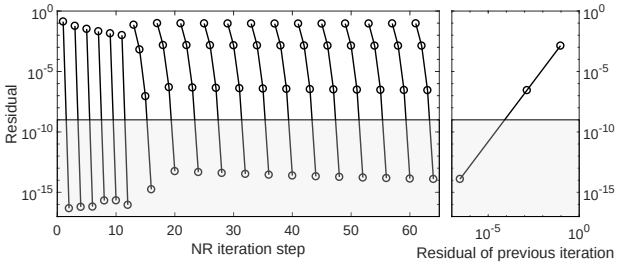

Figure 3: Left: The residual against the NR iteration step for each load-step, in which markers along a curve indicates NR iterations in that load-step, in the simulation with the sMPM. Right: The residual in the (n+1)-th iteration against that in the n-th iteration for the last load-step. The slope of two segments are 1.9951 and 1.9965, showing the convergence rate is quadratic.

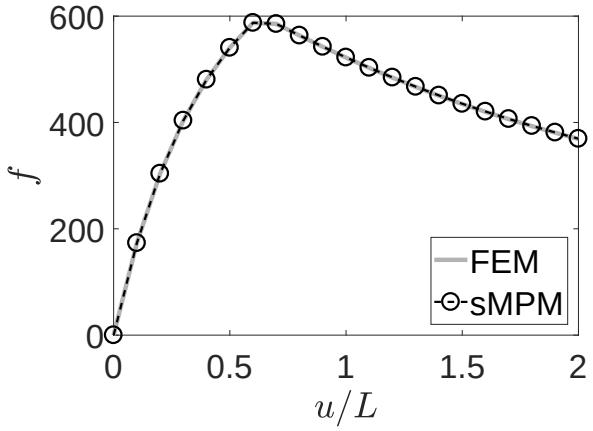

Figure 4: The reaction force on the right end of the block. The results from the CPDI approaches are the same with those from the sMPM.

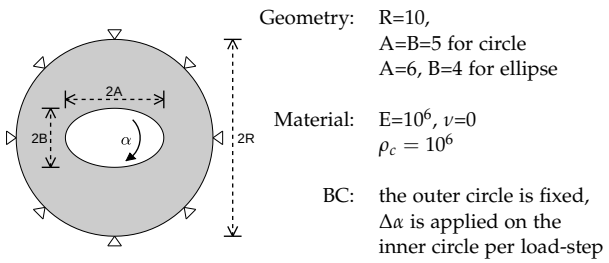

Figure 5: The geometry, material parameters and boundary conditions (BC) for the simulation of doughnut twist.

Two groups of simulation were carried out with circular and elliptical holes, respectively. Through these simulations, we are investigating:

1) the variation in response among the sMPM, CPDI approaches and FEM; and
2) the capacity of each method for modelling this large rotation.

In order to simulate this problem, the moving mesh was adopted as the rigid rotating mesh fixed to the inner circle or ellipse.

3.2.1 *Variation in response*

For question 1), the results from different methods when $\alpha = 10°$, i.e. small torsion, are first compared. In this case the deformed FE mesh suffers only minor distortion, thus the FE results are still reliable

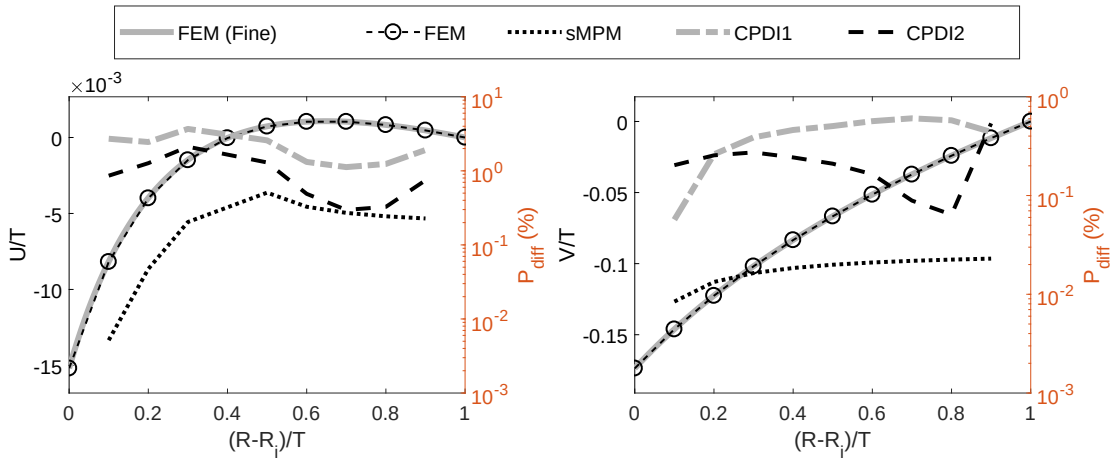

Figure 6: The two components of displacement across the wall of doughnut when $\alpha = 10°$. The displacements U, V are non-dimensionalised by the thickness of doughnut T. The FE results with both fine (160×1152 elements) and coarse (10×72 elements) meshes are plotted. The difference in the sMPM and CPDI approaches results to the FE results are shown on the right hand axes.

as a control. With the FEM, fine (160×1152 elements) and coarse (10×72 elements) meshes were used, in which the number before the sign $\times$ indicates the number of elements in the radial direction and the other is in the circumferential direction. The agreement of the results between fine and coarse meshes (Figure 6) suggests the coarse mesh is good enough for modelling this deformation. Therefore, this coarse mesh was used as computational mesh in the simulation with the sMPM and CPDI approaches. In all simulations, four material points per element were used. All simulations were run with the rotation increment $\Delta\alpha = 5°$ in the clockwise direction up to $\alpha = 10°$ in two load-steps.

The variations in response predicted by these methods are demonstrated by comparing the displacements along a radius (Figure 6) and the reaction force (Figure 7) on the inner circle during this simulation. The reaction force f is computed as the summation of the reaction force magnitudes at all nodes along the inner circle. The mesh nodes along the radius at the central angle $\theta = 0°$ were selected as sampling points, indicated by markers in Figure 6. From the FEM simulation, these nodal displacement were used directly. However, these sampling points have to be added as the material points in the sMPM and CPDI1 approach, in order to obtain comparable total displacements. These extra material points were also assigned a tiny square domain with edge length 0.001, for computing the initial volumes in the sMPM and for specifying particle domains in the CPDI1 approach. In contrast, the CPDI2 approach did not need these material points. Instead the displacements at corners of some particle domains were used. That is because the corners of some particle domains coincide with the sampling points in the initial configuration and these domains follow the deformation.

The difference in the displacement from the sMPM and CPDI approaches were computed with respect to

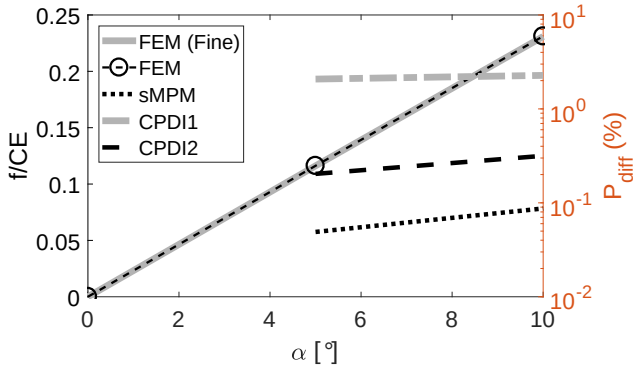

Figure 7: The normalised reaction force in FE simulation with fine and coarse mesh, and the difference in the sMPM and CPDI approaches results to the FE results. The force f is summation of reaction at all nodes along the inner circle, and C is circumference of the inner circle and E is the Young's modulus.

the FEM results as

$$P_{diff} = \frac{u^m - u^{FE}}{u^{FE}}, \tag{2}$$

where u^m is the displacement component from the sMPM and CPDI approaches and the superscript m indicates a method. The comparison in Figure 6 shows the CPDI1 approach to differ the most from the FEM result ($<$%5), followed by the CPDI2 approach($<$1%), while the sMPM is the most similar to the FEM ($<$0.05%). The difference in CPDI1 result and the FEM result is because the CPDI1 approach uses a parallelogram for a particle domain, and there are consequently overlaps and/or gaps among particle domains for covering this problem domain. The difference between the collection of these parallelogram particle domains and the actual deformed domain results in the difference in the stiffness matrix for simulation. In contrast, quadrilateral particle domains are employed in the CPDI2 approach, so avoiding this difference. The observation, that the results from the sMPM are closer to those from the FEM than from the CPDI2 approach, is because of the mapping of

displacement information between material point and mesh nodes, which needs to be done in two steps in the CPDI2 approach but only one in the sMPM. For example, updating of material points, positions at the end of a load-step needs: 1) interpolation of nodal displacements onto the corners of particle domains; and 2) computation of incremental displacements at material points based on the corners of their own particle domains. In the sMPM, the incremental displacement at material points is simply interpolated from the nodal incremental displacement.

3.2.2 *Capacity of methods for large torsion*

For question 2), all methods were applied to simulate the doughnut twist problem up to $\alpha = 80°$. The magnitude of reaction force along the inner circle against the boundary condition α is plotted in Figure 8. These reaction forces are almost the same in the elastic region when $\alpha < 25°$, but the FEM results are very different to the sMPM and the CPDI approaches in the plastic region when $\alpha > 30°$.

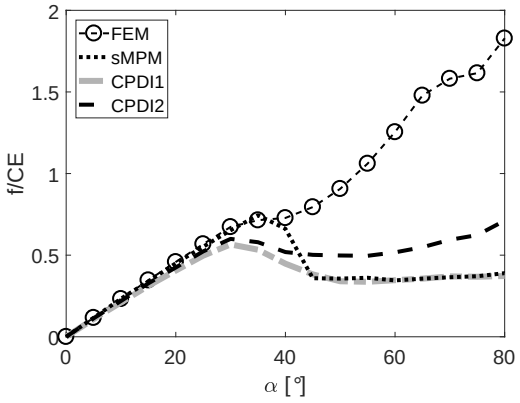

Figure 8: The normalised reaction force in the simulation with the same mesh (5×18 elements) in the FEM, sMPM and CPDI approaches.

When the material yields, the reaction force is expected to decrease, as observed in the results of the sMPM and CPDI approaches. The reaction force in the FEM is erroneously increasing due to errors brought via mesh distortion. Around $\alpha = 35°$, a larger peak was observed in the sMPM than in the CPDI approaches. The results of the sMPM are closer to those of the FEM than the CPDI approaches before $\alpha < 40°$ as demonstrated in the previous section. The drop following the peak appears to be due to the stress relaxation when the inner material yields while the external material is still elastic, as shown in Figure 9. The incremental displacements are shown for $\alpha = 30°$, $45°$ and $60°$. The first layer mesh nodes are rotated in the opposite direction–counter-clockwise to the boundary condition which is applied clock-wise on the inner circle when $\alpha = 45°$, showing the stress relaxation.

Both the sMPM and CPDI1 approaches predict the same constant reaction force for $\alpha > 50°$, but the CPDI2 approach has a slight increase. This erroneous increase is because of the distortion of particle domains. Recall that in the CPDI2 approach the particle domains exactly follow the deformation as in a FE mesh, but the distortion causes more serious error in the FEM than the CPDI2 approach.

The performance of these methods was also investigated through the simulation of doughnut twist with an elliptical hole. In these simulations, the mesh at the ends of the long axis were locally refined because the deformation gradient and stress tends to concentrate in these positions. The deformed mesh with incremental displacement and material points in the load-steps for $\alpha = 20°$, $30°$ and $60°$ are shown in Figure 10. Due to the stress concentration at ends of long axis of the ellipse, the material yields earlier than for a circular hole. As the ellipse further rotates in the plastic material, two regions with fewer material points are created after the ends of long axis passing, e.g. see Figure 10 when $\alpha = 60°$. The magnitude of torque against α in Figure 11 shows that the CPDI2 approach predicts erroneous increase in the plastic region again. Both the CPDI1 approach and the sMPM predict a more physically realistic response.

4 CONCLUSIONS

This paper has presented a common computational framework for the sMPM and its extensions, i.e. the CPDI approaches, which is first validated and then applied to problems involving large rotational deformation. In the published papers, the CPDI2 approach is the latest extension of the sMPM. Using the CPDI approaches can increase the stability of the computation, but as shown here can lead to erroneous results if the particle domains are distorted. As observed in the simulations of the doughnut twist problem, the increase in the torque predicted using the CPDI2 approach does not seem physically correct. The CPDI1 approach appears to have less negative effect on the results. In contrast, the sMPM predicts physically reasonable response, and stable reaction force and torque after the material is yielded. In the simulations for the doughnut with the circular hole, both the sMPM and the CPDI1 approach predict the same asymptotic reaction force, but for an elliptical hole they predict different values. Without referring to a reliable control, we cannot tell which is the closest to the exact solution. But both the sMPM and the CPDI1 approach predict what appear to be more physically reasonable responses than the CPDI2 approach. In practice, increasing the number of material points per element could improve the stability of the sMPM. In conclusion, the CPDI2 approach appears not to be suitable for simulating these large rotational problems.

ACKNOWLEDGEMENTS

We are grateful for the support by the UK Engineering and Physical Sciences Research Council grant (No. EP/N006054/1).

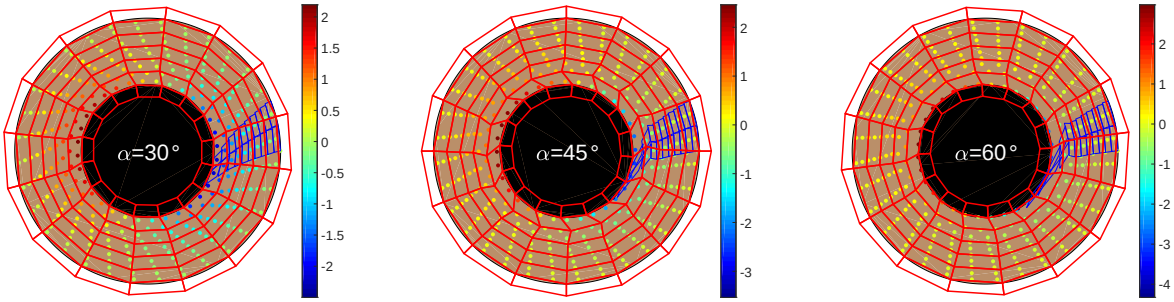

Figure 9: Deformed mesh at end of the load-step for $\alpha = 30°$, $45°$ and $60°$, with color on material points showing the total vertical displacement in the CPDI1 simulation. The blue lines show the particle domains.

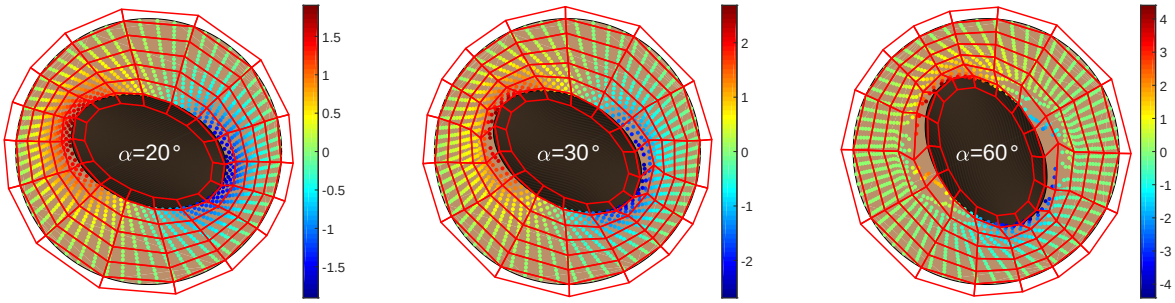

Figure 10: Deformed mesh at end of the load-step for $\alpha = 20°$, $30°$ and $60°$, with color on material points showing the total vertical displacement in the sMPM simulation.

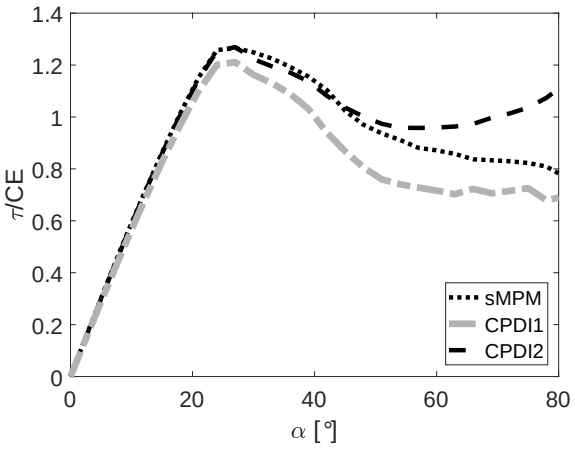

Figure 11: Normalised torque versus rotation α for the elliptical hole, where C is the circumference of the ellipse and E is the Young's modulus.

REFERENCES

Bardenhagen, S. & E. Kober (2004). The generalized interpolation material point method. *Computer Modeling in Engineering and Sciences 5*(6), 477–496.

Beuth, L. (2012). *Formulation and application of a quasi-static material point method*. Ph. D. thesis, University of Struttgart, Germany.

Ceccato, F., L. Beuth, P. A. Vermeer, & P. Simonini (2016). Two-phase material point method applied to the study of cone penetration. *Computers and Geotechnics 80*, 440–452.

Charlton, T., W. Coombs, & C. Augarde (2017). iGIMP: An implicit generalised interpolation material point method for large deformations. *Computers & Structures 190*, 108–125.

Coombs, W. (2011). *Finite deformation of particulate geomaterials: frictional and anisotropic Critical State elasto-plasticity*. Ph. D. thesis, Durham University, UK.

Cortis, M., W. Coombs, C. Augarde, M. Brown, A. Brennan, & S. Robinson (2017). Imposition of essential boundary conditions in the material point method. *International Journal for Numerical Methods in Engineering 133*(1), 130-152.

Nie, Y., Y. Li, & L. Wang (2012). Parallel node-based local tetrahedral mesh generation. *Computer Modeling in Engineering & Sciences(CMES) 83*(6), 575–597.

Sadeghirad, A., R. M. Brannon, & J. Burghardt (2011). A convected particle domain interpolation technique to extend applicability of the material point method for problems involving massive deformations. *International Journal for Numerical Methods in Engineering 86*(12), 1435–1456.

Sadeghirad, A., R. M. Brannon, & J. Guilkey (2013). Second-order convected particle domain interpolation (CPDI2) with enrichment for weak discontinuities at material interfaces. *International Journal for Numerical Methods in Engineering 95*(11), 928–952.

Wang, L., W. M. Coombs, C. E. Augarde, M. Brown, J. Knappett, A. Brennan, D. Richards, & A. Blake (2017). Modelling screwpile installation using the MPM. *Procedia Engineering 175*, 124–132.